PHYSICAL REVIEW B VOLUME 58, NUMBER 7 15 AUGUST 1998-I

Transient ion-drift-induced capacitance signals in semiconductors

T. Heiser*
Université Louis Pasteur, Laboratoire de Physique et Applications des Semiconducteurs, CNRS, BP 20, F-67037 Strasbourg Cedex 2, France

E. R. Weber
Department of Material Science and Mineral Engineering, University of California at Berkeley, Berkeley, California 94720
(Received 5 February 1998)

A theoretical model is developed that describes capacitance signals induced by drift of mobile ions in the space charge region of a Schottky diode. Pairing between the diffusing ion and the doping impurities is taken into account. The coupled partial differential equations are resolved numerically and the influence of key parameters on the signal shape is analyzed. Special emphasis is put on those features that enable transient ion-drift- (TID-) induced signals to be distinguished from capacitance transients caused by deep-level carrier emission processes. Relaxation kinetics and reverse bias dependence of the signal shape represent two reliable tools to verify the ion-drift nature of the signals. Methods for extracting quantitative information on both diffusion and pairing properties of the mobile ions are described. The question of whether pairing or diffusion is limiting the process is addressed. The influence of the doping level on the signal time constant is used to evaluate whether or not the diffusion is trap limited. A semiempirical model is described that permits the estimation of diffusion and pairing coefficients without resolving numerically the differential equations. Experiments are performed on interstitial copper in *p*-type silicon to test the predictions of the theoretical model. An overall agreement is found between theory and experiments. [S0163-1829(98)07331-7]

I. INTRODUCTION

Numerous mobile impurities have been reported to drift under strong electric fields in semiconductor devices. In the early 1960s, extensive Li drift studies were motivated by the need for high resistive materials to be used in nuclear detection.[1,2] More recently, atomic hydrogen in silicon was investigated by a large number of research groups (see Ref. 3 for a review). Hydrogen drift and diffusion were observed using capacitance voltage measurement in both *p*-type and *n*-type silicon.[4,5] Time-dependent capacitance signals occurring *during* ion drift were first reported by Johnson and Henning on hydrogenated silicon[6] and led to new data on the atomic hydrogen charge states and the corresponding deep levels in silicon.

Transition metals in silicon constitute another example of highly mobile defects in semiconductors. Drift of interstitial iron in silicon was studied by photocapacitance and deep-level transient spectroscopy (DLTS) measurements.[7] Due to the average neutral charge state of iron in the depletion region, this process was found to be limited by an electron emission step. Interstitial copper (Cu_i) is the fastest known diffusing impurity in silicon. It behaves as a shallow donor and forms acceptor-donor pairs.[8,9] Prescha *et al.*[10] used capacitance voltage measurements to observe Cu_i drift and study its diffusion and pairing properties below room temperature. Transient capacitance signals induced at room temperature by Cu drift in a *p*-type silicon Schottky diode were reported by Heiser and Mesli.[11] The copper drift process was fast enough to occur repeatedly when a low frequency reverse bias pulse was applied to the device. This so-called ''transient ion-drift'' (TID) method[11] was initially applied to study Cu_i diffusion properties over a large temperature range in the presence of acceptor-donor pairing. It was shown later that, when a high temperature anneal is followed by quenching the sample to room temperature, most copper atoms remain interstitially dissolved for several hours.[12] This result made TID analysis suitable for detecting low copper concentrations in silicon in the framework of contamination, gettering, or diffusion barrier studies.

Numerous highly mobile impurities exist in compound semiconductors as well. Ag and Cu in binary and ternary compounds were shown to diffuse over macroscopic distances even at room temperature and are of considerable technological importance for device applications.[13] Recently, Lyubomirsky, Rabinal, and Cahen used TID to study room-temperature diffusion properties of Ag, Li, and Cu in CdTe, $Cd_{0.7}Hg_{0.3}Te$, and $CuInSe_2$.[14]

Ion-drift-induced capacitance signals carry information about the diffusion properties and concentration of mobile impurities. If the mobile ion is involved in a reaction between defects, such as acceptor-donor pairing, the signals are influenced by the corresponding dissociation and capture rates as well. In Ref. 11, Heiser and Mesli derived an analytical semiempirical model to describe the ion-drift process and obtained a relationship between the transient capacitance time constant and the ion diffusion coefficient. The acceptor-copper pairing reaction was assumed to remain at local equilibrium, and was described by an effective diffusion coefficient. A more accurate model can be established by numerical resolution of the corresponding diffusion and pairing equations.

In the present work, a theoretical model is developed that describes in detail the origin and properties of ion-drift-induced capacitance transients. The influence of the diffusion coefficient, doping concentration, pairing constants, and ap-

 © 1998 The American Physical Society

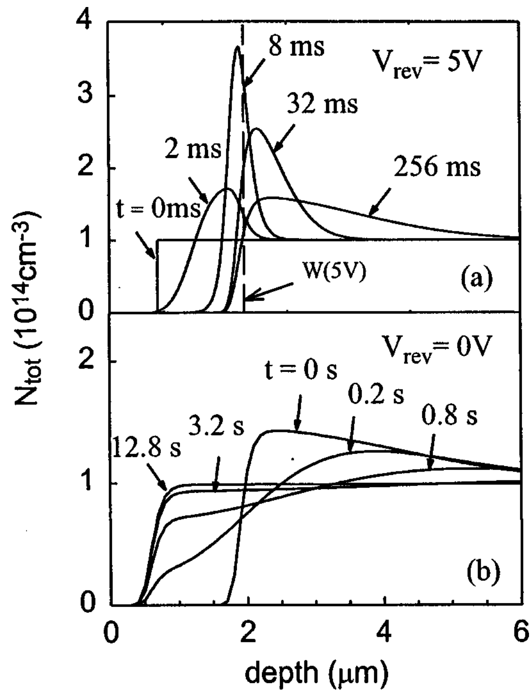

FIG. 1. (a) Calculated solute depth profiles after various drift periods at a reverse bias of 5 V. The dashed line represents the edge of the depletion region. (b) Relaxation profiles after several periods at 0 V. The initial profile was obtained after 1 s at 5 V. For both figures the parameters were taken as listed in Table I.

plied voltage on the shape of the signal is investigated. Special emphasis is put on those features that can be used to distinguish ion-drift-induced signals from more common deep-level carrier emission processes. The rate-limiting processes as well as the accuracy of the simplified analytical model are discussed. Interstitial copper in silicon is used as a model system to test the conclusions of the calculations. In particular, variously doped silicon samples are used to examine the influence of pairing on TID signals. A complete study of the copper-silicon system is, however, beyond the scope of the present paper.

The article is organized in five sections. Section II describes the origin of drift-induced capacitance transients and the related coupled partial differential equations. In Sec. III, numerical resolutions of these equations are given and the influence of major experimental parameters are discussed. Section IV describes TID measurements done on copper diffused and quenched silicon. Comparison between experimental and theoretical results is discussed in Sec. V.

II. THEORETICAL BACKGROUND

A. The origin of transient ion-drift signals

Transient capacitance signals are most commonly observed when the charge distribution inside the space charge region (SCR) of a Schottky diode, or equivalent device, is modified by emission from traps and subsequent drift of electrical carriers towards the bulk.[15] Due to the large carrier mobility, the last process is almost instantaneous. The resulting capacitance transients carry information only about physical properties of the defect, such as energy levels, defect concentrations, and carrier capture cross sections. In a like manner, the charge density can be altered when highly mobile ionized impurities are present in the SCR. The depletion capacitance will change when ion drift occurs. If the ion has the same charge as the majority carriers, the electrical field will drive it towards the neutral region, leading to a higher space charge density and a correspondingly higher capacitance. The ion redistribution, which occurs when a reverse bias is suddenly applied, is illustrated in Fig. 1(a). The curves have been obtained using the model discussed below. The process can be reversed if the bias voltage is reduced. Figure 1(b) describes how thermal diffusion leads to a quasiuniform ion distribution within the previously depleted region. Under a low-frequency reverse bias pulse and adequate duty cycle, the ions will engender a periodical back and forth movement, which in turn induces repetitive capacitance transients. The corresponding transient ion drift signals carry information on the effective mobility and concentration of mobile impurities. Temperature-dependent measurements yield activation energies, which in the case of a pure diffusion process, are equal to the defect migration enthalpy. However, if the ion is trapped along its diffusion path, then the activation energy of the ion drift process will be mostly determined by the trap binding energy. The concentration of the diffusion species is directly related to the signal amplitude, as will be discussed in Sec. III.

B. Differential equations

A better understanding of ion-drift-induced capacitance signals can be obtained by solving the coupled differential equations that govern the diffusion process. The model developed below describes the ion drift across a reverse biased Schottky diode, assuming a constant diffusion coefficient, D, a diffusion-limited trapping of the mobile ion (or solute) at the doping impurities, and a thermal dissociation of neutral solute-dopant pairs. We also assume that the majority carriers and solute ions carry the same electrical charge, that the background doping is uniform, and that the minority carriers and doping compensation by other impurities are negligible. Furthermore, it is assumed that Einstein's relation between the ion mobility μ and its diffusion coefficient holds.

The solute density $N_{\mathrm{sol}}(x,t)$ obeys the following equations:

$$N_{\mathrm{sol}}(x,t)=N(x,t)+P(x,t), \tag{1}$$

$$\frac{\partial N(x,t)}{\partial t}=\frac{\partial}{\partial x}\left[D\,\frac{\partial N(x,t)}{\partial x}+s\mu N(x,t)\frac{\partial V(x,t)}{\partial x}\right]-\frac{\partial P(x,t)}{\partial t}, \tag{2}$$

$$\frac{\partial P(x,t)}{\partial t}=4\pi R_c D N(x,t)[A_{\mathrm{tot}}-P(x,t)]-\nu P(x,t), \tag{3}$$

$$\frac{\partial^2 V(x,t)}{\partial x^2}=-\frac{q}{\varepsilon_s}\{N_{\mathrm{sol}}(x,t)-A_{\mathrm{tot}}+[A_{\mathrm{tot}}-N_{\mathrm{sol}}(L)]e^{-q[V(x,t)-V(L)]/kT}\}, \tag{4}$$

where $N(x,t)$ and $P(x,t)$ are the concentrations of unpaired and paired solute atoms, respectively, A_{tot} is the total doping density, $V(x,t)$ is the electrical potential distribution, R_c is the capture radius, ν is the dissociation rate, q is the ion

TABLE I. Parameters used for the calculation of solute profile and related capacitance transients except when otherwise specified.

Parameters	V_{pulse} (V)	V_{bi} (V)	V_{rev} (V)	A_{tot} (cm^{-3})	D ($cm^2\,s^{-1}$)	R_c (nm)	ν (s^{-1})	$N_{sol}(L)$ (cm^{-3})	T (K)
Values	0	0.6	5	2×10^{15}	3×10^{-8}	5	1700	10^{14}	300

charge, ε_s is the semiconductor dielectric constant, L is the sample thickness, k is the Boltzmann constant, s is the sign of the ion charge state, and T is the temperature. The backside solute density, $N_{sol}(L)$, is assumed to be time independent.

Equation (2) describes thermally activated diffusion and drift in the electric field and includes a recombination term to take pairing into account. Equation (3) represents the solute-dopant interaction with a diffusion-limited capture rate and Eq. (4) is the Poisson equation. For boundary conditions, we assume no solute flux on both sample surfaces and equilibrium of the pairing reaction on the back side surface. The latter assumption is accurate as long as the sample thickness L is considerably larger than the SCR width. The total constant voltage drop is given by $\Delta V=V(0)-V(L)=V_{bi}+V_{ext}$, where V_{bi} is the Schottky diode built-in voltage and V_{ext} is the externally applied bias. The potential origin is chosen at the sample backside surface [i.e., $V(L)=0$].

In TID measurements, the signal acquisition starts when the applied voltage is changed from V_{pulse} to V_{rev}, increasing the depletion region width. We consider that instant as the origin of the time scale. If the pulse voltage was applied long enough, the system has reached a stationary state at $t=0$. Negligibly few solute atoms are left inside the depletion region, while in the neutral region, a uniform solute density, in equilibrium with the pairing reaction, has been established. We may thus approximate the initial solute distribution, $N_{sol}(x,0)$, by

$$N_{sol}(x\leqslant W_{pulse},0)=0, \quad N_{sol}(x>W_{pulse},0)=\bar{N}_{sol}, \tag{5}$$

where W_{pulse} is the width of the SCR under V_{pulse}, with the pairing reaction at thermal equilibrium. $\bar{N}_{sol}$ is the average solute density in the bulk, which is equal to $N_{sol}(L)$ and taken to be lower than the doping level.

The ion distribution will affect the SCR width and hence the depletion capacitance $C(t)$. Baccarani *et al.*[16] have proposed an analytical model to derive the Schottky diode capacitance for arbitrary steep doping profiles. The model assumes an abrupt space charge edge but does not involve the identification of free carrier and doping depth profiles in the quasineutral region. Because a strong ion accumulation at the edge of the SCR may lead to a significant difference between both distributions, we used the Baccarani model to calculate the TID-induced capacitance signals. The depletion capacitance per unit area, $C(t)$, can be related to the solute density by

$$\Delta V=-\frac{1}{\varepsilon_s}\int_0^{W(t)} x\rho(x,t)dx$$

$$+\frac{kT}{q}\left\{\ln\left[\frac{\rho(W,t)}{\rho(L,t)}\right]-\frac{W(t)}{\rho(W,t)}\left.\frac{d\rho}{dx}\right|_{W(t)}-1\right\} \tag{6}$$

with

$$\rho(x,t)=q[N_{sol}(x,t)-A_{tot}] \tag{7}$$

and

$$C(t)=\frac{\varepsilon_s}{W(t)}. \tag{8}$$

$\rho(x,t)$ represents the space-charge density, and $W(t)$ the depletion width. The term between brackets in Eq. (6) takes into account the difference between free carrier and space charge distributions.

III. NUMERICAL RESOLUTION

In this section Eqs. (1)–(8) are resolved numerically as a function of the key experimental parameters. Two major issues that need to be addressed are the distinction between ion drift and electrical carrier-emission-induced capacitance transients and the estimation of physical properties of the mobile ion. In the first part of this section we calculate the solute depth profiles and corresponding capacitance transients as a function of experimentally adjustable parameters, such as the applied voltages and pulse length. The characteristic features that are derived can be used experimentally to identify the origin of the capacitance signal. In the second part, the influence of the physical properties of the mobile ion on the TID signals is investigated. The question of whether diffusion or pairing is the limiting process is addressed. Extraction of those parameters from the measured transients is discussed in the last part.

A. Characteristic features of TID signals

1. Depth profiles

Equations (1)–(4) were numerically solved using the finite difference method implemented in the software package ZOMBIE.[17] The parameters used are summarized in Table I. The capture radius was chosen typical for acceptor-donor pairs at room temperature,[1] while the dissociation rate was taken from measured values of Cu-B pairs.[10] The diffusion coefficient is chosen to fit approximately our experimental results discussed in Sec. IV. These values describe a relatively weak solute-dopant interaction, corresponding to about 20% of pairs at thermal equilibrium.[1] The ion distribution as a function of time under reverse bias is plotted in Fig. 1(a). A strong accumulation at the edge of the SCR is already observed after a few milliseconds. If subsequently the voltage is switched back to V_{pulse}, the ion redistribution occurs as shown in Fig. 1(b). The time required to reestablish a uni-

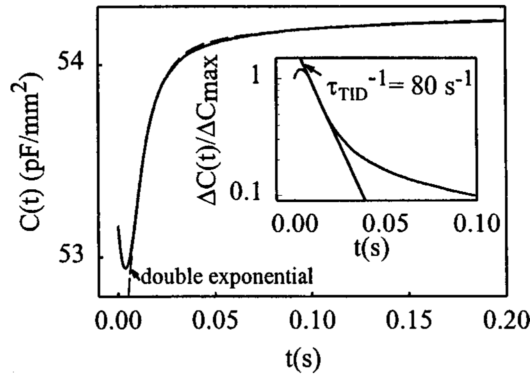

FIG. 2. Calculated ion-drift-induced capacitance transient using the parameters in Table I. The dashed line represents the double exponential function, $f(t)=54.28-2.13\exp(-t/0.01)-0.2\exp(-t/0.16)$. The inset represents a semilogarithmic plot of the normalized signal, defined by $\Delta C(t)/\Delta C_{\max}=[C(t)-C(t\rightarrow\infty)]/[C(0)-C(t\rightarrow\infty)]$, where $C(t\rightarrow\infty)$ was estimated at $t=5$ s.

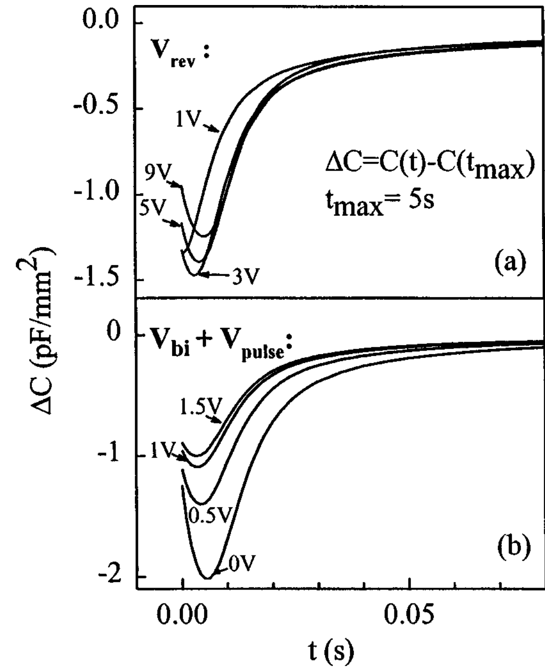

FIG. 3. Ion-drift-induced capacitance transients calculated either as a function of the applied reverse voltage (a), or as a function of the sum of built-in and pulse voltages (b). All other parameters are specified in Table I.

form solute distribution is significantly longer than the time needed for ions to drift out of the space charge region. Hence, in order to observe repetitive TID transients, the voltage ''pulse'' should be considerably longer than the time interval during which the capacitance transient is measured. The ''relaxation kinetics,'' which describes the signal amplitude as a function of pulse length, is discussed in detail in Sec. III A 4.

2. Transient capacitance signal

The corresponding time-dependent capacitance is calculated by numerically integrating Eqs. (6)–(8), and is shown as the solid line in Fig. 2. The capacitance first decreases slightly before it increases towards its stationary value. The figure insert represents the normalized curve plotted on a logarithmic scale. Following the initial capacitance decrease, a simple exponential dependence holds for almost 80% of the total amplitude. A qualitative explanation for this behavior can be found in the ion drift kinetics. It has indeed been shown in Ref. 11 that, when the diffusion term in Eq. (2) is neglected, the solute displacement across the SCR follows an exponential time dependence. This leads to an exponentially increasing accumulation at the edge of the depletion region, which in turn triggers the diffusion out of the SCR and increases the capacitance. Thus the drift kinetics limits the early stage of the process and leads to an exponential time dependence. Subsequent flattening of the solute profile by thermal diffusion gives rise to the significantly slower residual increase.

The origin of the initial capacitance decrease is related to the redistribution of the ions *inside* the depletion layer. It has been shown by Kukimoto, Henry, and Merritt[18] that, in the case of a reverse biased n^+p junction, or equivalent device, an excess positive charge $\Delta\rho(x)$ added to the background doping density induces a first-order capacitance change ΔC given by

$$\frac{\Delta C}{C}\approx-\frac{1}{W}\int_0^W\Delta\rho(x)\,\frac{x}{A^-}\,dx, \qquad (9)$$

where W is the SCR width, A^- the acceptor density at the edge of the depletion layer, and C the quiescent capacitance. From Eq. (9) it follows immediately that a displacement of positively charged ions inside the depletion layer towards the neutral region will decrease the capacitance. Hereafter, we will call this property the *capacitance depth sensitivity*. In DLTS analyses Eq. (9) describes the influence of the trap depth distribution on the measurement sensitivity. In turn, it can be seen from Eq. (9) that the absolute capacitance change $|\Delta C|$ decreases when the total excess charge in the depletion region is not constant. This explains the capacitance increase that occurs during ion diffusion out of the SCR. DLTS transients never exhibit the initial drop since the drift of free carriers out of the depletion layer is considerably faster than the emission rate. The ion-drift-induced capacitance signals, however, result from a combination of both the redistribution inside the depletion layer and the diffusion into the neutral region.

3. Reverse bias dependence

It is interesting to study how the reverse voltage ($V_{\rm rev}$) affects the signal shape, even though only a minor influence is expected. Indeed, for larger voltages, the increased SCR width tends to slow down the ion out-diffusion process, while the correspondingly higher electric field accelerates the ion drift by almost the same amount. The simulations, represented in Fig. 3(a), find the expected behavior to be true only after the minimum in capacitance has occurred. For shorter times, the magnitude of the initial capacitance decrease gains importance with increasing voltage. This feature can be understood in terms of the capacitance depth sensitivity. The strong concentration gradient at the edge of the SCR causes an ion diffusion current, which smears out the solute

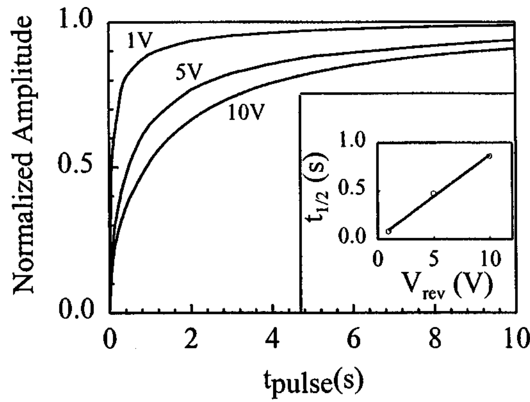

FIG. 4. Normalized amplitude of ion-drift-induced capacitance signals, defined by $\Delta C_{t_{\text{pulse}}}/\Delta C_{t_{\text{pulse}}\to\infty}$ with $\Delta C_{t_{\text{pulse}}}=[C(t\to+\infty, V=V_{\text{rev}})-C(t=0, V=V_{\text{rev}})]_{t_{\text{pulse}}}$ for three different reverse voltages as a function of the pulse length, t_{pulse}. The other parameters used are specified in Table I. The inset shows the time $t_{1/2}$, at which half of the maximum amplitude is reached, as a function of reverse voltage.

distribution inside the SCR. For a low reverse voltage, the SCR width is comparable to the accumulation layer extension and weakens the capacitance depth sensitivity. Conversely, for a high reverse voltage the overlap between the distribution inside and the accumulation profile at the edge of the SCR remains negligible during the initial stage of the drift process and increases the amplitude of the capacitance drop, as shown in Fig. 3(a). Likewise, the built-in and pulse voltages affect the initial capacitance decrease, since both parameters alter the depletion width during the pulse. Consequently, as indicated in Fig. 3(b), the initial capacitance decrease disappears for higher built-in and pulse voltages. Since both V_{rev} and V_{pulse} modify the signal shape, the bias dependence of the capacitance transient can be used to verify the ion drift origin of the signal.

4. Relaxation kinetics

Another characteristic feature of TID signals is obtained by measuring the relaxation kinetics, i.e., the signal amplitude versus pulse width. When the voltage pulse V_{pulse} is applied, the ion distribution ''relaxes'' by thermal diffusion towards a uniform distribution in the previously depleted region [see Fig. 1(b)]. The necessary time to reach the final distribution, or relaxation time, is of the order W^2/D, which is considerably larger than the TID time constant, and increases linearly with reverse voltage. Figure 4 shows the normalized signal amplitude as a function of the pulse length for three different voltages, using the parameter set of Table I. The inset indicates that the ''relaxation time,'' or the time necessary to reach half of the maximum amplitude, increases almost linearly with the reverse bias. The voltage dependence of the relaxation time is a characteristic feature for TID originating capacitance signals. Indeed, for deep-level carrier-emission-induced transients, which occur in DLTS analyses, the analog for relaxation is the carrier capture in the neutral region. This process should not depend on the electric field that existed in that region *prior* to the filling pulse. Hence monitoring the relaxation kinetics is a reliable way to distinguish between deep level carrier emission and ion drift induced capacitance signals.

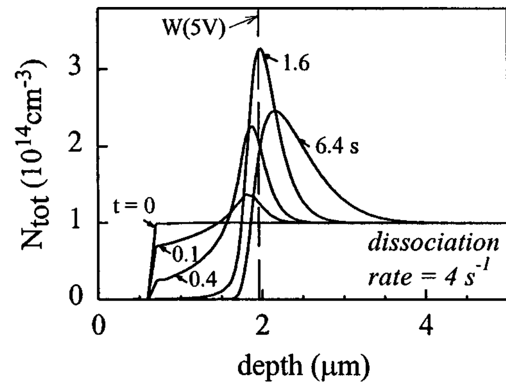

FIG. 5. Solute depth distribution calculated for a low dissociation rate, for which only 10% of the ions are unpaired. All other parameters are given in Table I.

B. Influence of pairing and diffusion properties

Once the origin of the signal is ascertained, the primary goal of TID analyses is the determination of physical properties relevant to the diffusion and defect reaction of the diffusing ion. To understand how these properties influence the signal shape, and under what experimental conditions they can be best estimated, we calculated the TID signal as a function of the diffusion and pairing constants. The results are summarized by way of an effective TID time constant, τ_{TID}, which is defined by the slope of the linear part of the signal represented in a semilogarithmic scale (see inset in Fig. 2). Another possible definition of τ_{TID} emerges when noting that the signal increase can be well adjusted to a double exponential function (dashed line in Fig. 2). The characteristic TID time constant corresponds then to the inverse of the smallest exponent, which turns out to be always 20% lower than the value obtained using the first definition. The second definition is useful when the signal offset cannot be accurately measured. Note, however, that Eqs. (1)–(8) do not enable an analytical derivation of the approximately double exponential time dependence.

1. Dissociation rate and capture radius

Solute-dopant pairing slows down the ionic diffusion significantly. Figure 5 shows the solute profiles calculated at various drift periods with a relatively low dissociation rate of $4s^{-1}$, all other parameter values being summarized in Table I. In this case only 10% of solute atoms remain unpaired at equilibrium. The profiles differ from those shown in Fig. 1(a) by more than just a time scaling factor. In particular, the concentration front, which is seen to drift towards the bulk in Fig. 1(a), is less apparent in Fig. 5. Thus, pairing is not satisfactorily portrayed by substituting D by a concentration independent *effective* diffusion coefficient in Eq. (2), as would be expected if the pairing reaction had reached local equilibrium during the drift process.[1] Note that the profiles in Fig. 5 are similar to the ion distributions measured by Prescha *et al.*[10] on Cu-diffused silicon using $C(V)$ analyses at temperatures where pairing dominated the process.

The solid lines in Fig. 6 represent the inverse TID time constant or TID rate, τ_{TID}^{-1}, as a function of the dissociation rate, for various capture radii. For low dissociation rates, τ_{TID}^{-1} increases linearly at a rate that depends only on the

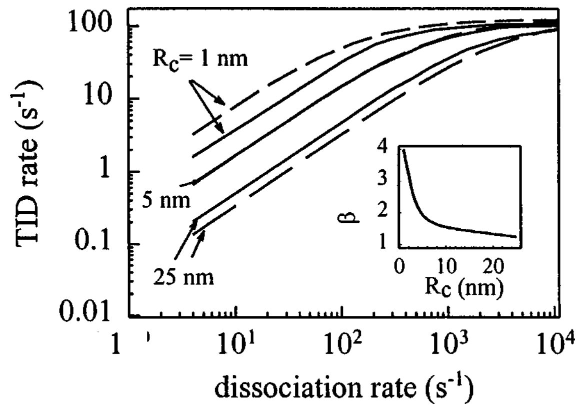

FIG. 6. The solid lines represent the TID rate as a function of solute-dopant pair dissociation rate, for different capture radii, calculated using the full theoretical model. All other parameters are specified in Table I. The dashed lines are obtained using the semiempirical model. The inset describes the variation of the correction factor β as a function of R_c.

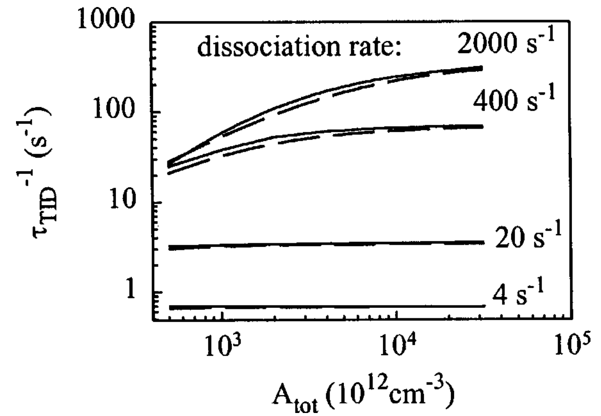

FIG. 7. The solid lines represent the calculated TID rate as a function of the doping density for different dissociation rates. All other parameters are specified in Table I. The dashed lines are obtained using the semiempirical model.

capture radius, indicating that pairing is the limiting process. At higher dissociation rates, τ_{TID}^{-1} saturates at a given value, which corresponds to the TID rate in the absence of pairing and is a function of the doping density and diffusion coefficient. The transition between the pairing and diffusion limited regimes occurs when τ_{TID}^{-1} is a few times higher than the dissociation rate, though the exact position where the transition occurs depends on the capture radius.

The initial capacitance decrease (not shown here) is lower in the case of stronger pairing due to the flatter ion distributions shown in Fig. 5. For low enough dissociation rates, the ion concentration decreases uniformly throughout the depletion region. Hence, as in carrier emission induced transients, the initial capacitance decrease is not observed. Consequently, the absence of a notable initial capacitance decrease in ion drift induced capacitance transients provides an indication that the diffusion is trap limited.

2. Doping density and diffusion coefficient

For constant reverse bias, higher doping densities induce stronger electric fields and hence faster ion drift kinetics. On the other hand, as the fraction of free solute ions is reduced with increasing dopant density, pairing will ultimately be the limiting factor of the process. The evolution of the TID signals as a function of doping density has been calculated for a constant solute to dopant ratio. The grid spacing used in the calculations had to be reduced with increasing doping level, in order to keep enough data points in the SCR and to avoid computational errors. The calculations are summarized in Fig. 7, where τ_{TID}^{-1} is plotted as a function of the doping concentration for different dissociation rates. For high dissociation rates, the TID rate increases almost linearly with A_{tot}, showing that the electric field enhancement of the drift kinetics is the dominant factor. For lower dissociation rates pairing is strong enough to keep the TID rate constant over the entire investigated concentration range.

A similar behavior is expected for the diffusion coefficient dependence of the TID time constant. Indeed, without significant pairing, drift inside the depletion region and subsequent diffusion towards the neutral region are the limiting processes. In this case, τ_{TID}^{-1} should increase with increasing diffusion coefficient. However, the diffusion limited capture rate increases with D and, ultimately, makes pairing the dominating process. Only a weak dependence on the diffusion coefficient is then to be expected. To test this statement, we calculated τ_{TID}^{-1} as a function of the diffusion coefficient for different dissociation rates. The solid lines in Fig. 8 represent the TID rate normalized by the dissociation rate as a function of the diffusion coefficient. The results indicate that τ_{TID}^{-1} increases almost linearly with D, as long as it is one order of magnitude lower than the dissociation rate. For higher diffusion coefficients, it reaches a limiting value τ_{max}^{-1} that depends on both dissociation rate and capture radius, and decreases with increasing fraction of paired ions in agreement with Fig. 6.

C. Estimation of physical parameters

Solute concentration and mobility, dopant-ion pair binding energy, and capture radius are the physical properties that are in principle accessible by TID analyses. The above investigations indicate, however, that strong pairing will allow

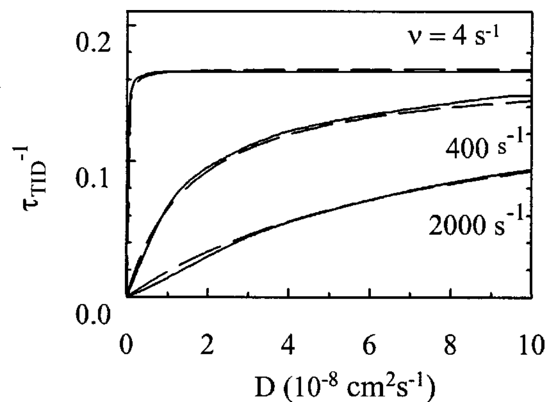

FIG. 8. The solid lines represent the calculated ratio between TID and dissociation rates as a function of the diffusion coefficient for different dissociation rates. All other parameters are specified in Table I. The dashed lines are obtained using the semiempirical model.

access to a lower limit of the diffusion coefficient only. In this case the TID rate is proportional to the dissociation rate and the temperature-dependent measurements provide information about the pair dissociation energy. In the case of weak pairing the linear dependence of $\tau_{\rm TID}^{-1}$ on D enables the ion migration enthalpy to be determined. Note, however, that all the numerical results discussed so far were obtained assuming a constant temperature. Yet, because the ratio between the mobility and diffusion coefficient decreases linearly with temperature, the TID rate should depend almost linearly on the temperature even when all other parameters are kept constant. Calculations of $C(t)$ as a function of temperature (not reported here) found indeed that $\tau_{\rm TID}T$ varies by less than 10% over temperatures between 200 and 400 K. Hence, the migration enthalpy can be extracted from temperature-dependent measurements, provided that $\tau_{\rm TID}T$ rather than $\tau_{\rm TID}$ is used in the Arrhenius plot. If the capture radius decreases linearly with increasing temperature, as it is the case for a Coulomb interaction,[1] and if pairing is dominating the process, no linear temperature dependence is observed. The pair binding energy should then be extracted from an Arrhenius plot of $\tau_{\rm TID}$.

Though the model presented above describes the fundamental mechanism of TID signal generation, it does not provide an analytical expression for extraction of the diffusion and pairing coefficients from experimental results. This may be achieved using a method based on the semiempirical model developed by Heiser and Mesli in Ref. 11. The model considers the ion ''time of flight'' across the SCR as the limiting process for TID.[11] When the diffusion term in Eq. (2) is neglected, the solute drift kinetics is described by an exponential time dependence with a time constant given by

$$\tau_{\rm TID}=\frac{W_{\rm rev}}{\mu E_M}=\frac{kT\varepsilon_s}{q^2DA_{\rm tot}}, \tag{10}$$

where E_M is the maximum electric field in the SCR. Each ion moves towards the neutral region according to

$$W-x(t)=[W-x(0)]\exp\left(-\frac{t}{\tau_{\rm TID}}\right), \tag{11}$$

where $x(t)$ represents the position of the ion at time t.[11,2] In the case of pairing, D is replaced by an effective diffusion coefficient, which at local equilibrium, is expressed by

$$D_{\rm eff}=\frac{D}{1+\Omega A_{\rm tot}}, \tag{12}$$

where Ω is the pairing constant.

Although the assumptions that diffusion is negligible and that pairing reactions are at local equilibrium are strictly speaking inaccurate, several properties of TID signals can be, at least qualitatively, deduced from Eqs. (10) and (12). A linear dependence of the TID rate on the diffusion coefficient and doping density is expected from Eq. (10) if pairing is negligible. In the case of strong pairing, a linear dependence between the TID rate and the dissociation rate is obtained when the pairing constant in Eq. (12) is replaced by

$$\Omega=\frac{4\pi R_cD}{\nu}. \tag{13}$$

Equation (13) holds under the assumption that the capture process is diffusion limited.[1,9] Moreover, if the product $A_{\rm tot}D$ is large enough, Eqs. (10), (12), and (13) lead to a TID rate that is independent of the doping density and diffusion coefficient. To achieve a quantitative agreement between both models, two dimensionless correction factors, α and β, need to be introduced into Eqs. (12) and (14). These equations are replaced by

$$\tau_{\rm TID}=\frac{\alpha kT\varepsilon_s[1+(4\pi R_cDA_{\rm tot}/\nu)\beta]}{q^2DA_{\rm tot}}, \tag{14}$$

with $\alpha=2.85$ and $\beta=1.95$. Results using Eq. (14) are plotted as dashed lines in Figs. 6–8 and agree well with the full theoretical model, except for the capture radii dependence. Both correction factors were chosen in order to yield the best fit for a capture radius of 5 nm (see Fig. 6). The physical meaning of α can be understood in terms of the drift kinetics. If thermal diffusion is neglected, each ion will see its position change according to Eq. (11). Equation (14) then represents the time needed by the ion to cover about 95% of its distance from the edge of the SCR. The necessity to introduce the second correction factor, β, is due to the inaccuracy of the local equilibrium assumption, which slightly underestimates the impact of pairing on the drift kinetics. Indeed, during the drift process, the unpaired ion and dopant densities become momentarily higher than the respective equilibrium values. The resulting larger capture rate is approximately taken into a account by introducing an effective capture radius $R_c^{\rm eff}=\beta R_c$. Whether or not the equilibrium approximation is physically sound depends on the capture radius. The larger the capture radius, the faster the pairing equilibrium is established and the lower the value of β needs to be. The behavior of β as a function of R_c is shown in the inset of Fig. 6.

The solute concentration in the bulk can be estimated from the TID signal amplitude, which is defined by $\Delta C=C(t\to+\infty,\ V=V_{\rm rev})-C(t=0,\ V=V_{\rm rev})$. For $\bar{N}_{\rm sol}<A_{\rm tot}$, an approximate relationship can be obtained analytically by resolving the Poisson equation for the two following solute distributions:

$$N_{\rm sol}(x)=\begin{cases}0 & \text{for } x<W_{\rm pulse}\\ \bar{N}_{\rm sol} & \text{for } x\geqslant W_{\rm pulse}\end{cases} \tag{15}$$

and

$$N_{\rm sol}(x)=\begin{cases}0 & \text{for } x<W_{\rm rev}\\ \bar{N}_{\rm sol} & \text{for } x\geqslant W_{\rm rev},\end{cases} \tag{16}$$

where $W_{\rm pulse}$ and $W_{\rm rev}$ are the SCR widths under $V_{\rm pulse}$ and $V_{\rm rev}$, respectively. The slight increase in the average solute concentration in the neutral region, following the drift-diffusion process, is negligible for a large sample thickness ($L\gg W_{\rm rev}$).

Finally,

$$\frac{\bar{N}_{\rm sol}}{A_{\rm tot}}=\frac{C_\Delta^{-2}-C_h^{-2}}{C_\Delta^{-2}-C_l^{-2}}, \tag{17}$$

where $C_h = C(t\to\infty)$, C_l is the stationary capacitance at V_{pulse} and $C_\Delta = C_h - \Delta C$. In the case of $\bar{N}_{\mathrm{sol}} \ll A_{\mathrm{tot}}$, and for $V_{bi} + V_{\mathrm{pulse}} \ll V_{\mathrm{rev}}$, expression (17) reduces to the well-known relation[15]

$$\frac{\bar{N}_{\mathrm{sol}}}{A_{\mathrm{tot}}} = 2\frac{\Delta C}{C_h}. \tag{18}$$

Expression (17) agrees well with the numerical resolution of Eqs. (1)–(8). The solute density affects only weakly the signal shape, as long as it is significantly lower than the doping concentration.

IV. TID ON Cu CONTAMINATED *p*-TYPE SILICON

A. Experimental details

The different features of ion-drift-induced capacitance transients, discussed in the previous section, can be tested on Cu in-diffused and quenched silicon. Copper in silicon is known to have a high interstitial diffusivity.[8] Though interstitial copper solubility is almost negligible at room temperature,[8] a significant amount of copper atoms remain interstitially dissolved if a high temperature anneal is followed by a rapid quench.[12] Moreover, interstitial copper behaves as a donor and forms pairs with acceptors by Coulomb interaction.[9,10] Prescha *et al.*[10] have measured the dissociation rates of copper-acceptor pairs and have found a significant lower binding energy of B-Cu pairs as compared to Al-Cu, Ga-Cu, or In-Cu pairs.[10] We take advantage of this particular feature to evaluate the influence of pairing on the TID signals.

In this work we used boron-, aluminum-, and gallium-doped Czochralski-grown silicon- and boron-doped float zone silicon, provided by Wacker Chemitronic, with resistivities ranging from 0.1 to 20 Ω cm. After removing the native oxide by 50% HF, a thin copper layer was deposited by dipping the samples into a $CuF_2\cdot 3H_2O/HF/H_2O$ (10 g/10 ml/500 ml) solution. The HF component of the above solution prevents significant oxide growth between the Cu film and the silicon surface, which can act as an in-diffusion barrier. The samples were annealed at 650 °C for 2 h, followed by quenching into ethylene-glycol and storage in liquid nitrogen. After chemically removing the surface layer and etching the samples in a $HNO_3/HF/CH_3COOH$ (2.7/1/1) solution, a thin Al film was evaporated to form Schottky diodes. Ohmic contacts were obtained by Ga eutectic plating on the sample backside. Low contact resistivities were achieved by scratching the back surface with a diamond tip. Capacitance transients were measured at room temperature using a commercial DLTS setup. The standard voltage pulse parameters were $V_{\mathrm{rev}} = 5\,V$, $V_{\mathrm{pulse}} = 0$. The pulse duration was set to 9 s for B-doped silicon and 90 s for Ga- and Al-doped material. The signal amplitude did not increase with longer pulse widths, indicating that the initial quasi-uniform Cu distribution was reached after each pulse.

B. TID results

1. Reverse bias dependence

Capacitance transients, measured at different reverse voltages on 0.1 Ω cm B-doped silicon, are presented in Fig. 9.

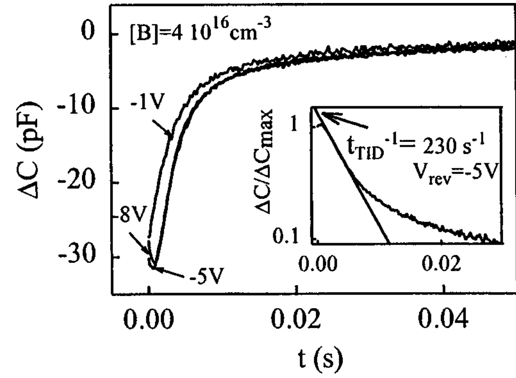

FIG. 9. Experimental TID transients measured at room temperature on Cu contaminated B-doped silicon for different reverse voltages. The inset represents a semilogarithmic plot of the normalized signal, defined by $\Delta C(t)/\Delta C_{\mathrm{max}} = [C(t) - C(t\to\infty)]/[C(0) - C(t\to\infty)]$, where $C(t\to\infty)$ was estimated at $t = 5$ s.

The characteristic initial capacitance decrease is clearly seen and depends strongly on the applied reverse voltage. Yet its amplitude is smaller than expected from the calculations and differs from one diode to the other. For low copper concentrations it is hidden by the signal noise. We attribute this behavior to the fluctuations of the Al diode barrier height and to the non-uniform carrier profile in the near surface layer. $C(V)$ measurements indicated a strong decrease of the acceptor concentration close to the surface due to acceptor passivation by atomic hydrogen-introduced during chemical processing of the semiconductor surface. The zero bias SCR width was of approximately 1 μm. Although the non-uniform doping was not taken into account in the calculations, it is possible that it reduces the magnitude of the initial decrease in capacitance. Finally, the initial rectangular solute distribution used in our simulations [see Eq. (5)] slightly overestimates the capacitance at $t = 0$. Similar measurements were performed on 1-Ω cm Al-doped material and the results are shown in Fig. 10. The two orders of magnitude larger TID time constant is ascribed to the higher Al-Cu binding energy as compared to B-Cu pairs. Again, the capacitance drop increases with voltage in agreement with calculations.

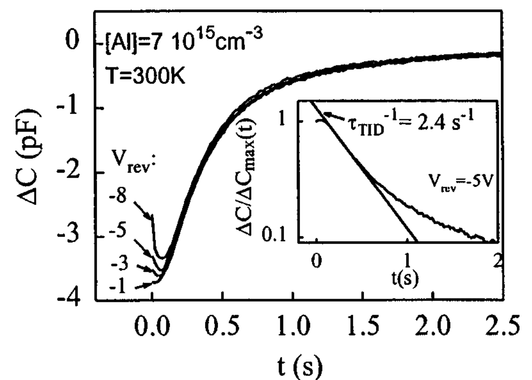

FIG. 10. Experimental TID transients measured at room temperature on Cu contaminated Al-doped silicon for different reverse voltages. The inset represents a semilogarithmic plot of the normalized signal, defined by $\Delta C(t)/\Delta C_{\mathrm{max}} = [C(t) - C(t\to\infty)]/[C(0) - C(t\to\infty)]$, where $C(t\to\infty)$ was estimated at $t = 50$ s.

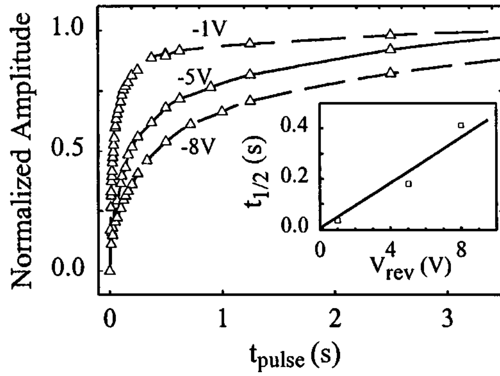

FIG. 11. Relaxation kinetics measured at room temperature on B-doped silicon for three different reverse voltages. The inset shows the time $t_{1/2}$, at which half of the maximum amplitude is reached, as a function of reverse voltage.

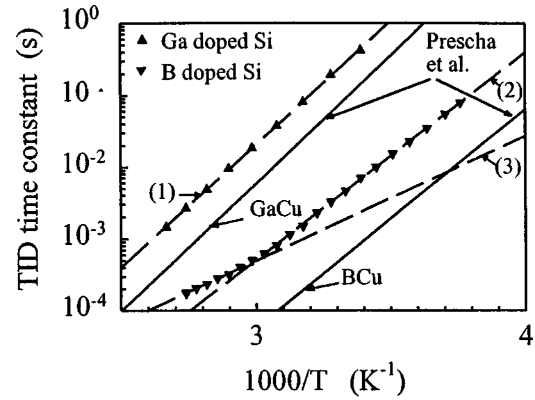

FIG. 12. Temperature dependence of the TID time constant, τ_{TID}, measured on B- or Ga-doped silicon. Also shown are the inverse dissociation rates for Ga-Cu and Ga-B pairs, as determined by Prescha *et al.* (Ref. 10) and given by $\nu_{GaCu}^{-1} = 1.3\times10^{-13}\exp(0.71\pm0.02\ \mathrm{eV}/kT)$ and $\nu_{BCu}^{-1} = 3.8\cdot10^{-14}\exp(0.61\pm0.02\ \mathrm{eV}/kT)$. The dashed lines represent exponential functions that fit best to our experimental results. The corresponding activation energies are $\Delta E_{Ga}=0.68\pm0.02$ eV (curve 1), $\Delta E_{B1}=0.58\pm0.02$ eV (curve 2), and $\Delta E_{B2}=0.35\pm0.02$ eV (curve 3).

2. Relaxation kinetics

Relaxation kinetics, measured in B-doped silicon for different reverse voltages, are shown in Fig. 11. Note that the filling pulse, required to reach 95% of the maximum signal amplitude, is of the order of seconds. In the case of Al or Ga doping, stronger pairing makes the required pulse length exceed 1 min. These values are significantly larger than typical deep-level pulse widths ($<200\ \mu$s) and constitute by themselves a characteristic feature of ion-drift-induced capacitance transients. The measured kinetics slow down as expected when the voltage bias is increased. The relaxation time $t_{1/2}$ closely follows the expected linear voltage dependence (see figure inset). To our knowledge, no electrical carrier emission phenomenon has been observed that could lead to a similar voltage dependence.

The TID signal shape is almost independent of the relaxation time, except for its amplitude and initial drop. This behavior, which is consistent with the theoretical model, indicates that the quasiexponential capacitance increase is governed by the strong accumulation at the edge of the SCR and subsequent out-diffusion, rather than by the ion profiles inside the depletion region. A similar behavior has already been reported by Johnson and Henning[6] in the case of atomic hydrogen drift-induced transients.

3. Temperature and doping dependence

We performed temperature-dependent measurements on both B-doped and Ga-doped materials. As the activation energies for migration and pair dissociation are different, the influence of pairing is expected to change with temperature. Capacitance transients were measured at various temperatures between 265 K to 365 K and the corresponding Arrhenius plot of τ_{TID} for both dopants are represented in Fig. 12. Also shown are the dissociation data from Prescha *et al.*[10] In the Ga-doped material, τ_{TID} follows a straight line over the whole temperature range with an activation energy of 0.68 ± 0.02 eV, which is close to the Ga-Cu dissociation energy of 0.71 eV.[10] The unique slope of the Arrhenius plot indicates that, for Ga-doped Si, copper-gallium pairing dominates the process over the whole accessible temperature range, i.e., between 295 and 375 K. For B-doped material, a change of slope is observed around 330 K. At temperatures below 330 K, the process is described by an activation energy of 0.59 ± 0.02 eV, which agrees well with the Cu-B dissociation energy of 0.61 eV reported by Prescha.[10] In this temperature range, the B-Cu pairing limits the Cu drift process. Above 330 K the slope of the experimental curve decreases and the activation energy drops down to 0.35 ± 0.02 eV. If the linear temperature dependence of τ_{TID} in the absence of pairing (see Sec. III C) is taken into account, this value becomes 0.37 ± 0.02 eV. Yet, the narrowness of temperature range (340–365 K) from which this energy was determined allows only the conclusion that this value is an *upper* limit of the migration enthalpy. The slope change in the Arrhenius plot of τ_{TID} represents the transition between the trap-limited and diffusion-limited TID process. A more complete study of copper impurities in silicon is beyond the scope of the present article.

Temperature-dependent expressions for the Ga-Cu and B-Cu pair dissociation rates can be obtained from the results shown in Fig. 12, using Eq. (14) under the assumption of strong pairing, i.e., when the value of the diffusion coefficient D is not needed. If the capture radius decreases linearly with temperature and is equal to 5 nm at room temperature, the dissociation rates are described by

$$\nu_{GaCu}=5.2\times10^{12}\exp\left(-\frac{0.68\pm0.02}{kT}\right)\ \mathrm{s} \tag{19}$$

and

$$\nu_{BCu}=5.4\times10^{12}\exp\left(-\frac{0.58\pm0.02}{kT}\right)\ \mathrm{s}, \tag{20}$$

which are close to the values reported by Prescha *et al.*[10]

The influence of pairing can also be seen by measuring TID signals as a function of acceptor concentrations. The experimental results obtained for B-doped, Al-doped, and Ga-doped silicon are summarized in Fig. 13. Similar TID rates are found in Ga-and Al-doped Si and are almost inde-

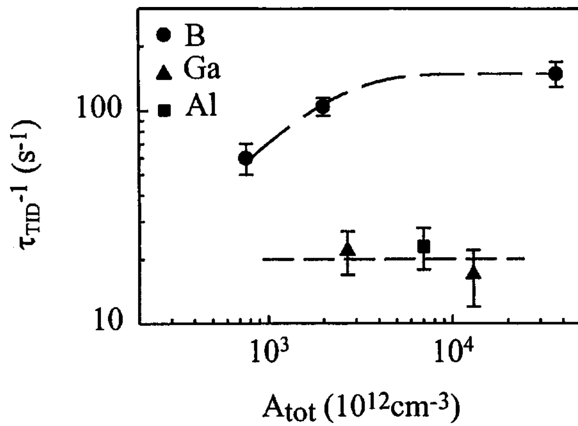

FIG. 13. Room-temperature TID rates measured in B-, Ga-, and Al-doped silicon of different resistivities. The dashed lines outline the behavior of the TID rate vs doping level with a constant dissociation rate.

pendent on the Ga density. This behavior is consistent with the matching binding energies of Al-Cu and Ga-Cu pairs and the resulting similar dissociation rates.[10] The significantly lower B-Cu binding energy, however, causes a two orders of magnitude higher dissociation rate. In this case the TID rate increases with doping density as expected for weak pairing (see Sec. III B 2).

V. DISCUSSION

From the theoretical calculations developed in Sec. II, several signatures of ion-drift-induced capacitance transients appear to be of importance when the origin of the signal is to be discussed. Extended pulse lengths, which are required to observe signals, and a nonexponential capacitance transient are two properties that are unexpected but not excluded for a deep-level carrier emission process. The presence of an initial capacitance decrease, the magnitude of which depends on the voltage pulse, is a more specific signature of TID signals, though the amplitude of the signal decrease often appears to be lower than expected from theory. A large zero bias depletion width, which in silicon is often due to hydrogen in-diffusion during processing, could explain this discrepancy in magnitude. Efficient pairing that flattens the solute profiles in the SCR, reduces the capacitance depth sensitivity and the magnitude of the initial capacitance decrease as well. The initial capacitance dip has also been observed by Lyubomirsky[14] on Cu contaminated CdTe crystals. The authors suggested that a chemical reaction of defects involving copper was at the origin of the capacitance decrease. If the decrease is found to be more pronounced for higher reverse voltages, the capacitance depth sensitivity should also be considered as a possible origin of the observed behavior.

The relaxation kinetics discussed above are the most reliable way to identify the ion drift origin of the signal. No other physical process, which could give rise to a similar voltage dependence, has been reported so far. The voltage dependence of the relaxation time constant, Fig. 13, can be used even for relatively low solute densities when the capacitance decrease is barely observable.

An overall agreement is obtained between theoretical results discussed in Sec. III and experimental data collected on the Cu diffused and quenched silicon. The capacitance transients observed at room temperature for Cu diffused B-doped, and Ga- or Al-doped silicon, have a two orders of magnitude difference in the respective time constants. Yet, they both show the characteristic TID features: initial capacitance drop and voltage-dependent relaxation kinetics. Therefore they can be confidently ascribed to the same physical process, namely, interstitial copper ion drift.

Pairing affects the TID signal considerably. The calculations show that information on solute diffusivity can only be obtained if the TID rate is significantly larger than the pair dissociation rate, while only a lower limit of the diffusion coefficient can be estimated in the opposite case. The activation energies obtained from temperature-dependent TID measurements described in Sec. III confirm this assertion. A similar situation has been reported on H drift experiments by Zundel and Weber.[19] The question of whether or not pairing is limiting the process can be settled by performing TID measurements on samples with different resistivities. The TID rate is expected to be almost independent of the doping level if pairing is strong enough. TID can then be used to get information on the solute-dopant interaction.

Defect reactions involving species other than doping impurities are not included in the model. However, other defects present in the material might trap the solute impurities and affect the TID signal as well. For instance, the TID signal amplitude observed in Cu diffused silicon decreases when the samples are left at room temperature for several hours.[12] We believe this behavior is due to clustering or precipitation of interstitial copper.[20] As a consequence, precipitation kinetics can be monitored by TID and information on the density and capture radius of nucleation sites can be obtained.[21]

VI. CONCLUSION

The numerical resolution of the coupled diffusion, pairing and Poisson equations have led to a fundamental understanding of the ion drift induced capacitance signals. Several characteristic features of TID signals provide means to differentiate ion-drift-induced capacitance transients from signals produced by more common electrical carrier emission processes. The model refines the description of the influence of solute density, diffusion coefficient, and pairing constants on the signal shape. It shows in particular that, in the case of strong pairing, the signal shape becomes almost independent of the ion mobility, so that only a lower limit of the diffusion coefficient can be estimated. TID signals depend then strongly on the pair dissociation rate, providing information on the pairing reaction. For weak pairing, the diffusion coefficient influences the signal shape significantly and enables the temperature-dependent ion mobility to be determined from experiments. A semiempirical model is proposed to allow the estimation of the diffusion and pairing coefficients without resolving numerically the differential equations. The influence of defect reactions involving species other than the

dopant on TID signals are beyond the scope of the present article. Nevertheless, the issue may be of interest for studying the physics of defect interactions. Several physical systems in which ion drift induced capacitance transients occur have been described in the literature. Some have a considerable technological impact. For instance, the high sensitivity of transient capacitance measurements makes TID a potential technique for monitoring low level copper concentrations in silicon in the framework of diffusion barrier and gettering studies, as well as in contamination control issues.

ACKNOWLEDGMENTS

We would like to thank K. Knobloch, A. Istratov, C. Flink, H. Hieslmair, A. Mesli, and A. Golanski for stimulating discussions, E. Edelson and C. Eckert for their valuable comments on the manuscript, and P. Yam for his technical support. The use of the Lawrence Berkeley National Laboratory experimental facilities that are funded through the DOE is also acknowledged. The present work has been supported by the Wafer Engineering and Defect Science Consortium and the UC MICRO program.

*Electronic address: Heiser@phase.c-strasbourg.fr

[1] H. Reiss, C. S. Fuller, and F. J. Morin, Bell Syst. Tech. J. **35**, 535 (1956).
[2] P. Baruch, J. Appl. Phys. **32**, 653 (1961).
[3] S. J. Pearton, Int. J. Mod. Phys. B **8**, 1093 (1994).
[4] T. Zundel and J. Weber, Phys. Rev. B **39**, 13 549 (1989).
[5] C. H. Seager, R. A. Anderson, and D. K. Brice, J. Appl. Phys. **68**, 3268 (1990).
[6] N. M. Johnson and C. Herring, Phys. Rev. B **46**, 15 554 (1992).
[7] T. Heiser and A. Mesli, Phys. Rev. Lett. **68**, 978 (1992).
[8] R. H. Hall and J. H. Racette, J. Appl. Phys. **35**, 379 (1964).
[9] A. Mesli and T. Heiser, Defect Diffus. Forum **131**, 89 (1996).
[10] T. Prescha, T. Zundel, J. Weber, H. Prigge, and P. Gerlach, Mater. Sci. Eng. B **4**, 79 (1989).
[11] T. Heiser and A. Mesli, Appl. Phys. A: Solids Surf. **57**, 325 (1993).
[12] T. Heiser, S. Mchugo, H. Hieslmair, and E. R. Weber, Appl. Phys. Lett. **70**, 3576 (1997).
[13] L. Chernak, K. Gartsman, D. Cahen, and O. M. Stafsudd, J. Phys.Chem. Solids **56**, 1165 (1995).
[14] I. Lyubomirsky, M. K. Rabinal, and D. Cahen, J. Appl. Phys. **81**, 6684 (1997).
[15] P. Blood and J. W. Orton, *The Electrical Characterization of Semiconductors: Majority Carriers and Electron States* (Academic Press, London, 1992), pp. 371–380.
[16] G. Baccarani, M. Rudan, G. Spadini, H. Maes, W. Vandervorst, and R. Van Overstraeten, Solid-State Electron. **23**, 65 (1980).
[17] W. Jungling, P. Pichler, S. Selberherr, E. Guerrero, and H. W. Potzl, IEEE Trans. Electron Devices **ED-32**, 156 (1985).
[18] H. Kukimoto, C. H. Henry, and F. R. Merritt, Phys. Rev. B **7**, 2486 (1973).
[19] T. Zundel, and J. Weber, Phys. Rev. B **46**, 2071 (1992).
[20] A. A. Istratov, C. Flink, H. Hieslmair, T. Heiser, and E. R. Weber, Appl. Phys. Lett. **71**, 2121 (1997).
[21] H. Hieslmair, C. Flink, S. McHugo, A. A. Istratov, and E. R. Weber, Mater. Sci. Forum **258–263**, 449 (1997).